ACCOUNTS
of chemical research

Peptide-Targeted Diagnostics and Radiotherapeutics

MICHAEL F. TWEEDLE

Departments of Radiology, Chemistry, and Pharmacy; The Ohio State University; Biomedical Research Tower; 460 West 12th Avenue, Columbus, Ohio 43215

RECEIVED ON SEPTEMBER 29, 2008

CONSPECTUS

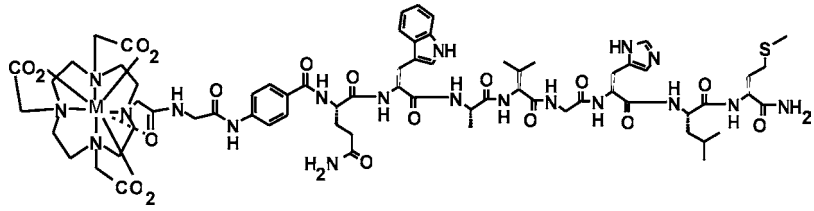

Radiotherapeutic drugs and medical imaging agents, although used for different purposes, both benefit from precise targeting. When systemically administered, either would be most useful if designed to find and bind only a tumor, single type of cell, or unique molecular assembly thereon. In this Account, we examine the use of small peptides, natural and synthetic, to create biochemically specific molecular imaging agents and radiotherapeutic pharmaceuticals, discussing three distinct examples.

In one project, a small natural peptide known to target members of the bombesin family of receptors was chemically attached to a strong, versatile metal chelator, DO3A, through a series of small-molecule linkers. The linkers powerfully affected not only binding strength for the bombesin receptors, tissue distribution, and tumor uptake *in vivo* but also receptor subtype specificity. When the assembly is combined with an active metal ion for human trials, the versatility of the DO3A (dodecanetriacetate) chelate affords choices in selecting the metal ion for different purposes: lutetium for a combination radiotherapeutic and diagnostic agent, ^{177}Lu-AMBA, and gallium for a positron emission tomography (PET) imaging agent, ^{68}Ga-AMBA.

We also created small (~5-kDa) bivalent peptides, each composed of different chemically linked peptides derived from phage display. The monomer peptides bound to the same target protein, VEGF-R2, a primary target of vascular endothelial growth factor (VEGF), the angiogenesis-stimulating protein. Several families of the monomer peptides did not compete with one another for the binding site on VEGF-R2. Their combination into fully synthetic hetero-bivalent molecules yielded subnanomolar K_d values and greater than 100-fold improvements over homo-bivalent molecules. Biological activity was evident in the hetero-bivalents, whereas none or very little existed in homo-bivalents, monomers, and monomer mixtures.

In ultrasound imaging, tiny bubbles (2 μm in diameter) filled with inert gas can be used as effective contrast agents. By coating the shell of such bubbles with the peptide TKPPR (a tuftsin antagonist), we created contrast agents that bound unexpectedly to cultured endothelial cells expressing angiogenesis targets; the binding was attributable to a previously unnoticed and powerful multivalency effect. TKPPR binds specifically to neuropilin-1 (NP-1), a VEGF co-receptor, but only when multimerized is it avid. Tuftsin, a small peptide derived from immunoglobulin G (IgG) that binds to macrophages during inflammation, has been studied for over 30 years; the receptor has never been cloned. Our results led to new conclusions about tuftsin, NP-1, and the purpose, heretofore unknown, of exon 8 in VEGF, which appears to be involved in NP-1 binding.

Our disparate projects demonstrate that small-peptide targeted molecules can be very versatile in drug discovery in combination with classical medicinal chemistry. In particular, multivalent interactions can lead to unpredictable and useful biochemical information, as well as new drug candidates.

Introduction

The ideal characteristics of systemically administered diagnostic imaging agents and radiotherapeutics differ somewhat. Both are ideally localized immediately after administration with maximum target/background ratio, high target uptake, and rapid excretion of untargeted drug. Imaging drugs are then expected to wash out of the target rap-

Published on the Web 06/24/2009 www.pubs.acs.org/acr
10.1021/ar800215p CCC: $71.50

idly after imaging, while radiotherapeutics ideally remain in the target (e.g., a tumor) for the radionuclide's useful lifetime to allow the radiation to destroy the target.

Our strategy for creating biochemically targeted imaging and radiotherapeutic pharmaceuticals also considers commercialization, which disfavors (in our view) very long circulation times due to potential toxicity (radiotherapeutics) and inconvenience (for diagnostics, long background clearance times). We also favor soluble entities over insoluble "nanoparticles" whenever possible. Proteins, antibodies, and macromolecular constructs are more difficult to reproduce, control, and register commercially, although they are often easier to use in research laboratories. Without ignoring the possibilities of macromolecular constructs, especially as ultrasound (US) agents, we developed a program to identify small molecule and peptide-targeted diagnostics and radiotherapeutics, a portion of which will be described herein.

DO3A

Many of the useful radionuclides are metals and so require metal-chelating agents to chemically attach them to their targeting moieties (e.g., peptides). For the metals that we have employed (lanthanides, In^{3+}, and Ga^{3+}), the tetra-aza-cyclododecanes have proven especially useful. The first unsymmetrically substituted chelators of this class, called DO3A (dodecanetriacetates) were created by the author and his colleagues at E.R. Squibb and Sons in the 1980s.[1] At that time, the symmetrical parent, DOTA (dodecanetetraacetate) had been discussed in the context of imaging by Gries,[2] Desreux,[3] and Sherry,[4] Desreux being the first to note its remarkable stability for the lanthanides, reporting binding characteristics even greater than that of the venerable lanthanide chelator, DTPA (diethylenetriaminepentaacetate). The discovery that the parent, unsubstituted DO3A molecule was still remarkably stable absent one of its carboxylate arms was made while researching impurities isolated during the synthesis of DOTA. The great stability and especially inertia to metal dissociation is now thought to be due to preorganization for metal chelation and has led to widespread use of DOTA and DO3A in molecular imaging, generally as unsymmetrically substituted derivatives targeted with biologically or chemically active moieties.[5,6] A Scifinder search of the substructure, DO3A, substituted unsymmetrically with three acetate arms and one nonacid arm, returned over 800 articles. While the cyclen-based chelators are best suited to the larger, tripositive lanthanide ions, they are also strong binders of Ga^{3+}. ^{68}Ga being an excellent isotope PET imaging, the choice of the DO3A chelator was an efficient one for screening and commercial development of both ^{177}Lu radiotherapeutics and ^{68}Ga diagnostic agents.

GRP-R Agents

Certain members of the gastrin-releasing peptide receptor family of high-affinity seven-transmembrane proteins in the G-coupled receptor superfamily are overexpressed on human prostate, breast, and lung cancers. A high-affinity binding ligand, bombesin (BBN), is a naturally occurring amphibian tetradecapeptide first isolated from the skin of a European frog. The BBN-related binding peptides, GRP and neuromedin B (NMB), are mammalian homologues. Four subtypes of the BBN-related peptide receptor have been described: GRP-R (BB2, BRS-2), NMB-R (BB1, BRS-1), the orphan receptor bb3 (BRS-3), and the amphibian receptor bb4. The C-terminal octapeptide BBN[7−14] is sufficient for the specific binding interaction with GRP-R and NMB-R, the two target receptors overexpressed on cancers, and it has been used in the context of imaging and radiotherapy. We started with this truncated octapeptide and attached it, through a series of chemical linkers, to DO3A, finally arriving at the AMBA ligand and its family of metal derivatives: Lu-AMBA, Hf-AMBA, Ga-AMBA, etc. (Figure 1). ^{177}Lu-AMBA, currently a clinical candidate radiotherapeutic, is a combination radiotherapeutic and diagnostic, by virtue of this isotope's medium range β and imageable γ radiation (β = 498/149 keV (max/avg), $t_{1/2}$ = 6.7 d; γ = 208 keV (11%) and 113 keV (6.4%)). ^{68}Ga-AMBA contains only a positron-emitting nuclide for PET imaging. The latter pharmaceutical could be used with ^{177}Lu-AMBA for patient selection or response monitoring or as a pure imaging agent.

^{177}Lu-AMBA

^{177}Lu-AMBA[7a−e] was created from the truncated peptide and the DO3A chelate, varying the linking group through parallel synthetic methods, creating milligram amounts and screening for binding to the target.[7e,8] Purity and identity were established at a screening level using HPLC and mass spectral analysis. Radiolabeled (usually with ^{177}Lu) and unlabeled compounds were screened against ^{125}I-BBN (universal ligand binding all GRP-R subtypes) in cultured human prostate cancer cells. We found similar binding behavior of the metal-containing and metal-free compounds, so we could screen the free compounds for receptor binding strength. This procedure was enough to choose ~10% of the hundreds of candidates to go on to limited normal mouse biodistribution to evaluate pharmacokinetics. A similar percentage of these candidates were discarded due to unacceptably fast or slow elimination. Elim-

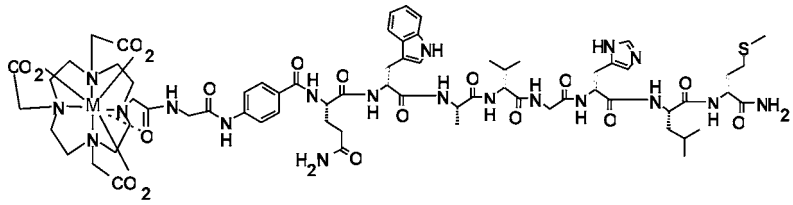

DO3A Linker QWAVGHLM-NH_2

Peptide		binding (IC_{50} in nM) NMB-R	GRP-R
Neuromedin B	GNLWATGHFM-NH_2	0.37±0.04	73±9
GRP	nGRP(1-17)GNHWAVGHLM-NH_2	0.90±0.03	0.56±0.04
Universal Ligand	^{125}I-yHWAV-βAla-HF-Nle-NH_2	0.23±0.01	0.62±0.07
BBN8: DO3A-CH_2CO-8-Aoc-QWAVGHLM-NH_2		0.42±0.01	0.74±0.12
8-Aoc = 8-aminooctanoic acid			
AMBA: DO3A-4-aminobenzoyl-QWAVGHLM-NH_2		0.51±0.04	0.21±0.08

FIGURE 1. Structures of GRP radiopharmaceuticals: homology of the peptide ligands of the GRP receptor family and structure of the M-AMBA family.

ination rates approximately within the glomerular filtration rate (through kidney to urine) with minimal hepatobiliary elimination (through liver to gut) were the crude initial target. The relative radiation toxicity to various radiation-sensitive organs like bone marrow and kidney (dosimetry) was modeled based on biodistribution and pharmacokinetics studies. Bone marrow radiation was quite low for the rapidly excreted compounds we sought. On the basis of expected dosimetry, we decided that the key features were the highest 24 h tumor retention (for maximal killing) and the lowest 24 h kidney retention. The remaining compounds were screened in a PC3 (human prostate cancer metastasis cell line) xenograft mouse tumor model for tumor uptake and retention. This reduced the total to 5, which were chosen in part for high tumor retention and low kidney retention at 24 h in tumor. Peptides tend to be sequestered and retained by kidney, a very radiosensitive organ, which leads to radiation toxicity to the kidney. These five candidates were compared with one another and a more lipophilic starting compound[9] (BBN8 in Figure 1) for radiotherapeutic efficacy over 30 days in the xenograft PC3 mouse model. Two final candidates (both relatively hydrophilic) were tested in a 120-day radiotherapy trial in the same animal model at a single 750 μCi dose to choose the final candidate, Lu-AMBA. A 120-day therapeutic trial survival curve in mice is shown in Figure 2. The data demonstrate not only effectiveness (>20% with no visible tumor after 120 days) of a single dose against this PC3 tumor but also the added effectiveness of two doses.

Pharmacokinetics were found to be linker dependent. ^{177}Lu-AMBA had the best retention of radioactivity in tumor vs kidney, along with rapid excretion of 60% of the dose into urine, where patients could eliminate it readily, as compared with more lipophilic compounds, which tended to have more liver uptake. Table 1 shows some key biodistribution data for Lu-AMBA demonstrating high tumor retention, low liver vs urinary excretion, and washout from kidney. Metabolism studies of Lu-AMBA in mouse, rat, and humans showed rapid cleavage of the peptide in plasma and mouse kidney homogenates with no parent compound excreted in urine.[10]

In addition, for unknown reasons, receptor subtype specificity was greatly affected by the linker. (Linker−tryptophan ring stacking was recently found.[11]) In mouse biodistribution, pancreas uptake was especially high for all of the compounds with high tumor uptake, but the efficacy studies on mice were not limited by the high pancreas uptake, a radioresistant organ. Pancreatic subtypes in mouse and human are expected to be different in favor of lower uptake in the human. This was borne out in the eventual human imaging dosimetry trial, preliminary data from which suggest extremely high human dose tolerance, >1 Ci of ^{177}Lu with pancreas as the target (dose-limiting) organ, and remarkably low kidney uptake and retention, especially considering the peptidic nature of the drug.[11]

Table 2 shows the linker used in AMBA compared with one where the aromatic group is moved slightly and the effect of this change on target binding. NMB-R and GRP-R are the subtypes known to be overexpressed on human tumor tissue samples. Not only do the absolute K_d values differ with this subtle change in structure, but also the relative receptor subtype binding changes significantly.[11]

Further biological studies on the main candidates were also conducted in preparation for human clinical trials. These included quantitative receptor binding measurements, cell

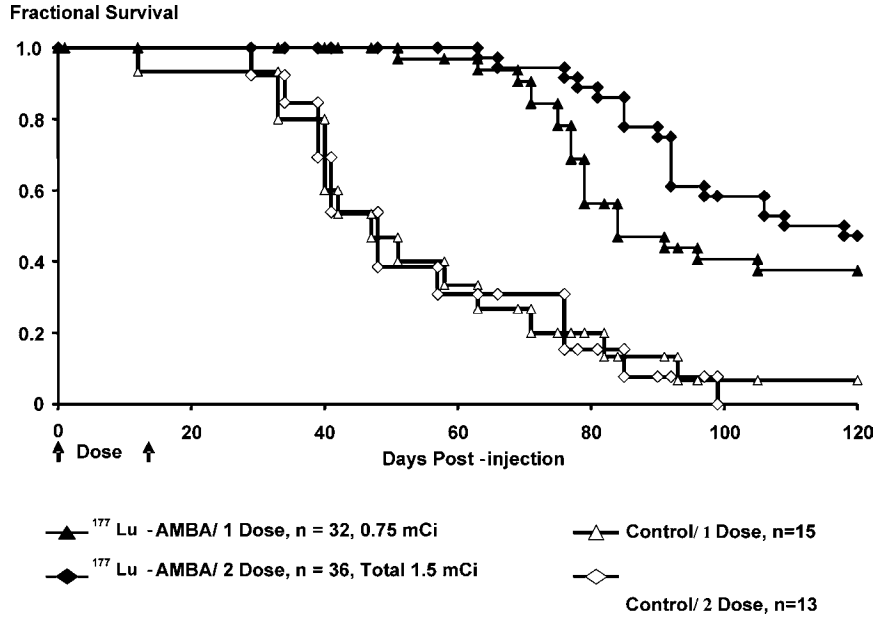

FIGURE 2. Therapeutic efficacy in PC3 xenograft mice given single and two 750 μCi doses of ^{177}Lu-AMBA, shown as Kaplan-Meir plots.

TABLE 1. Biodistribution Data for ^{177}Lu-AMBA in Xenograft PC3 Mice Administered as 5 μCi Dose[7a]

organ	% ID[a]/g tissue at 1 h	% ID[a]/g tissue at 24 h
tumor	5.0 ± 1.4	3.40 ± 0.95
liver	0.22 ± 0.11	0.39 ± 0.57
kidney	7.6 ± 2.9	2.69 ± 0.63
pancreas	50 ± 13	41.5 ± 7.9
blood	0.25 ± 0.13	0.02 ± 0.01
urine/bladder (% ID[a]/organ)	61.2 ± 8.1	

[a] Injected dose.

TABLE 2. K_d Values for Binding of Ligands as in Figure 1[a]

Linker	NMB-R	GRP-R
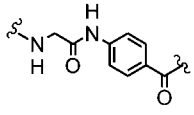	0.51 ± 0.04	0.21 ± 0.08
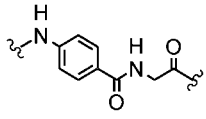	3.3 ± 0.2	20 ± 2

[a] After Swenson.[8]

studies to evaluate uptake and retention amounts and kinetics, detailed rodent biodistributions, plasma stabilities, decomposition pathway in kidney homogenates, imaging, and further efficacy studies.

Radiostability of ^{177}Lu-AMBA[7b]

One stringent chemical requirement of radiotherapeutics is high radiostability of the formulation. Isotope decay in concentrated manufacturing batches and even single patient dose levels causes highly destructive radicals that attack the vulnerable peptide, as shown in the HPLC trace inset in Figure 3. This was overcome through the use of stabilizers including a novel one, selenomethionine. This latter additive was imagined to protect the peptide's terminal methionine, which is important for receptor binding.

The interesting issue of the fate of ^{177}Lu-AMBA on radioactive decay was recently addressed by Cagnolini.[12] The ^{177}Lu decay produces stable Hf(IV). Hf(IV) starting materials did not react with AMBA ligand in water, so a stable Hf(IV)-AMBA was prepared by reaction of $HfCl_4$ with AMBA under nonaqueous conditions and it was fully characterized. Two interconverting isomers of unknown structure, visible on HPLC, coeluted with the products formed when ^{177}Lu-AMBA decayed for 43 d (~6 half-lives). Approximately 80% of the ^{177}Lu isotope decayed to stable Hf(IV) without the metal ion leaving the chelate, suggesting a remarkably radiation-stable chelate given the high recoil energy expected of the decay. It might be hypothesized that on decay, the Hf moves to a sitting-on-top complex (bound only to the charged oxygens), then re-enters the chelate, but the rate-limiting step for metal entry into cyclen-based chelates *is* the drop into the pocket.[13]

^{68}Ga-AMBA

Substitution of the positron-emitting ^{68}Ga creates a novel PET agent for imaging the presence or absence of GRP-R. The biodistributions of ^{68}Ga-AMBA and ^{177}Lu-AMBA are nearly identical. While this may seem unexpected given the smaller size and lower coordination number of Ga^{3+} compared with Lu^{3+}, rigidity and preorganization of DO3A probably makes the

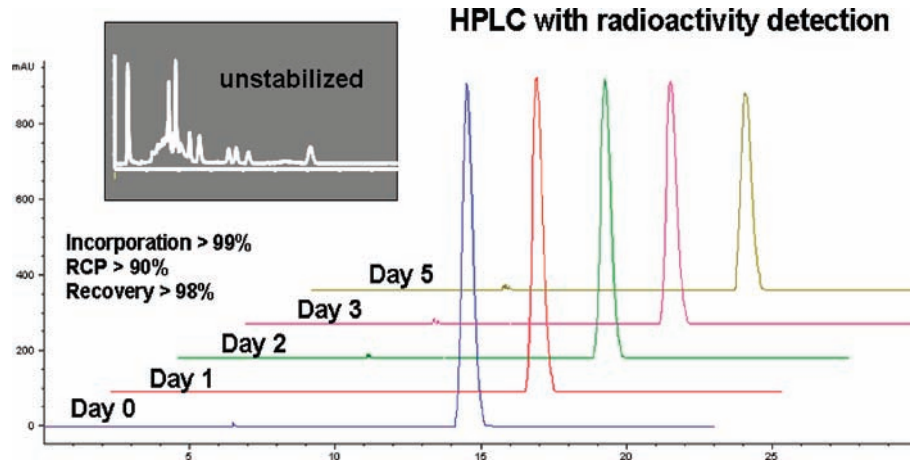

FIGURE 3. Radiodetected HPLC traces of formulations of ^{177}Lu-AMBA containing selenomethionine. Inset is an unprotected formulation at ~12 h.

structures similar. Use of Ga-AMBA would allow the use of PET (positron detection) rather than SPECT (gamma detection) for greater spatial resolution and quantitation.

Hetero-bivalent Peptides

Natural small peptides like GRP with 1−10 nM K_d values for target binding are rare. More often in drug discovery, one has a target that requires a ligand. While antibodies are well-known to have the required low K_d values, their binding strength comes largely from their bivalency and tertiary structure, so reducing them to smaller fragments (ScFv < 25 kDa) sacrifices K_d for smaller size, and the smaller size is seldom small enough to distribute and excrete pharmacokinetically like a "small molecule" (i.e., ≤5 kDa). We imagined creating synthetic, water-soluble molecules with size <5 kDa that bound targets with K_d =1−10 nM (i.e., a good pharmaceutical lead).

Small molecule drugs (≤1 kDa) can sometimes be created with the desired binding and pharmacokinetic properties, but these are generally made via arduous medicinal chemistry campaigns. When successful, they are usually lipophilic and frequently lack an innocent chemical structural element for attaching a diagnostic reporter. If a region of the molecule uninvolved in target binding is available for attaching a reporter, the ≤1 kDa size still means that that common diagnostic labels like metal chelates, ~0.4 kDa, are similar in size to the targeting ligand and will tend to interfere sterically with binding. One solution is to create ~5−10 kDa polypeptides that are still small enough to distribute and excrete like small molecule drugs. Specific binding peptides can be discovered de novo within billion-member "libraries" using phage display technology.[14] The binding strength of de novo phage display examples has, however, tended to be low (K_d ~100−1000 nM), requiring lengthy optimization campaigns.

An important, well-validated target in molecular imaging of cancer is angiogenesis, the process by which tissues generate new blood vessels. In angiogenesis, cancer cells, usually hypoxic and in need of a blood supply, secrete ligands (e.g., VEGF, vascular endothelial growth factor, a tyrosine kinase) that stimulate blood vessels' endothelial cells to bud and migrate toward the cancer cells, forming new capillaries. Drugs that bind to the natural angiogenesis receptor on endothelial cells, VEGF-R2, need to be powerful binders to compete with natural VEGF−VEGF-R2 binding in vivo ($K_d \approx 1$ nM). Concentrations of VEGF in vivo during angiogenesis are also high and active VEGF-R2 relatively low. All of this makes a powerful targeting ligand necessary.[15]

With the aim of eventually attaching new targeting peptides to diagnostic imaging agents, we used phage display to create small peptide binders to an Fc-fusion−VEGFR-2 construct. Initial screening was done with the isolated specific phage particles. Then peptides corresponding to the successful phage clones were synthesized. The peptide binders generated were single loop or linear peptides (<20-mers) with K_d values from tens of micromolar to 1000 μM affinity for VEGF-R2. They were screened using fluorescence polarization or surface plasmon resonance (SPR). Table 3 contains the K_d data for a set of first library monomers (rows 1 and 2). A second library, new viral particles created around the consensus sequences from the first library, produced monomeric peptides with K_d as low as 3 nM (row 3, -GGGK-NH_2, added as a linker, has little or no effect on binding).[16]

TABLE 3. K_d Values for Peptides Binding to VEGF-R2[a]

monomeric peptides	K_d (nM)
(1) Ac-GDSRVCWEDSWGGEVCFRYDPGGGKNH$_2$	70
(2) Ac-AGPKWCEEDWYYCMITGTGGGKNH$_2$	280
(4) Ac-AGPTWCEDDWYYCWLFGTGGGKNH$_2$	3
homo-bivalent (4) + (4)	5
homo-bivalent (1) + (1)	185
hetero-bivalent (1) + (2)	0.6
hetero-bivalent (1) + (4)	0.6

[a] Bivalents were linked as in Figure 5. K_d was measured by fluorescence polarization for monomers and SPR (Biacore) for bivalent molecules.[16]

While 3 nM is low enough for K_d, very few examples with K_d's approaching 3 nM occurred and none of them competed effectively with the natural ligand, VEGF, at accessible in vivo concentrations, ≤100 nM. Interestingly, the peptides tended to belong to one of two consensus sequence families that did not compete with one another for VEGF-R2 binding. This led us to conclude that we might increase affinity and effectiveness by creating hetero-multimers.

We therefore made tetrameric constructs using biotinylated conjugates of the binding peptides. Biotin is a small molecule (144 Da) that binds to avidin (60 kDa) with stoichiometry of 4:1 biotin/avidin and with a first $K_d \approx 10^{-15}$ M. We made tetramers of different peptides by stoichiometrically labeling the avidin with biotinylated peptides, making two series of tetramers: homo-tetravalents (all four peptides the same) and hetero-tetravalents (different peptides). The analytical assay was comparative binding to cells that had been transfected to overexpress VEGF-R2 vs binding to control cells, mock-transfected and not overexpressing VEGF-R2. The results are in Figure 4. The bars are transfected on the right of each pair and mock-transfected on the left. The tetramers tested are described below the bar with a number for each peptide on the avidin. For example, from left to right, the first tetramer contained 0 nonbinding peptide, 4 binding peptide A, and 0 binding peptide B. The next tetramer to the right contained 1 nonbinder, 3 binder A, and 0 binder B. The left-most four homo-tetravalents show that binding to the VEGF-R2-expressing cells increased as the number of copies of the binder A increased from 1 to 4. The same trend with a smaller magnitude was observed for the weaker binder B. Interestingly, the hetero-tetravalents with peptides from two noncompeting families showed a dramatic synergistic effect. Even hetero-tetravalents with two nonbinders possessed significant binding. We then created synthetically accessible heterovalents to reduce the size to <5 kDa. The structure and synthetic route to these are exemplified in Figure 5.[17]

Further binding results are shown in Table 3. Remarkably, the hetero-bivalents demonstrated 100−300-fold enhancement over the homo-bivalents, yielding K_d <1 nM. Twelve target proteins, similar and dissimilar to VEGF-R2, were tested against the monomers and heterovalents with negative binding, ruling out nonspecific binding. The heterovalents but not monomers or homovalents actively interfered with autophosphorylation of VEGF-R2 by VEGF in cultured endothelial cells with IC_{50} values at or near their K_d values.[16] Mixtures of both monomers (unconnected by chemical links) were inactive, like the homo-bivalents. Bio-

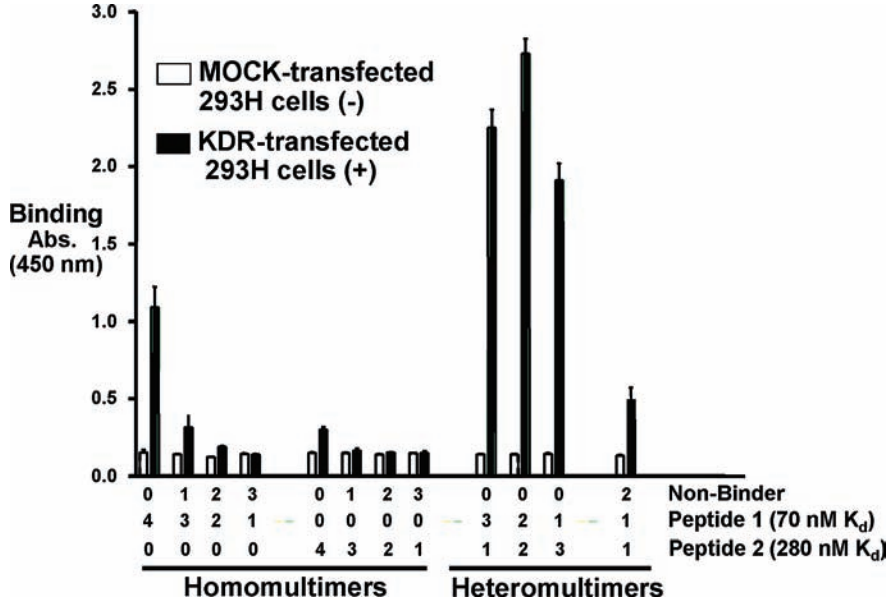

FIGURE 4. Cell binding results for homo- and hetero-tetramers of biotinylated peptides with avidin.[16] In the homo-tetramer series, binding increases with more binding vs nonbinding peptides in the tetramer. Hetero-tetramers show much stronger binding than homo-tetramers.

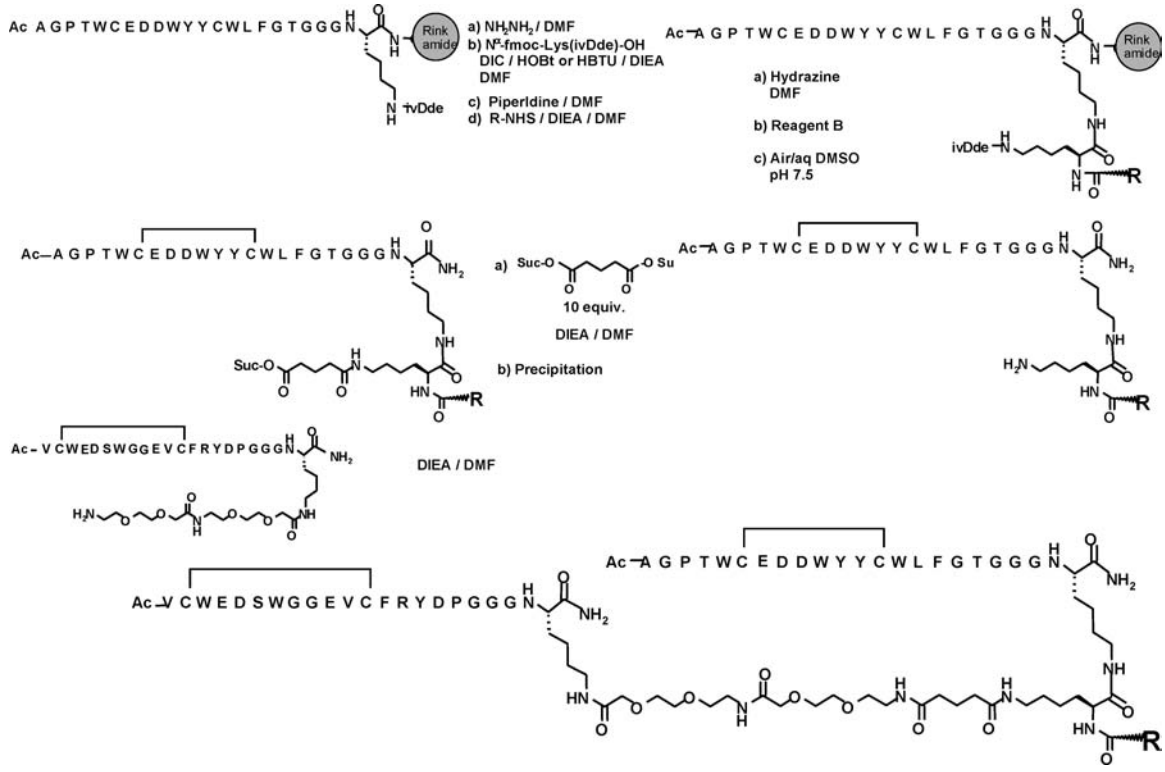

FIGURE 5. Synthetic scheme to create peptide herero-bivalent ligands.

logic activity assays were also positive for the ability of the hetero-bivalents to inhibit endothelial cell migration stimulated by VEGF. For example, hetero-bivalent 1 + 4 (K_d = 0.5 nM) had an IC_{50} of 1 nM in this assay, while monomer 4 (K_d = 3.2 nM) showed an IC_{50} of 800 nM. Taken together, the results indicate that hetero-bivalency confers both high binding strength and biologic activity.

A second tyrosine kinase, C-Met (high-affinity receptor for hepatocyte growth factor) was also used to generate hetero-bivalent molecules from its phage display hits and gave the same results as those for VEGF-R2, yielding again $K_d < 1$ nM,[16] leading us to conclude that the formula is a general one, at least for tyrosine kinases.

The structure of the hetero-bivalents proved to be chemically tolerant. The linker is unsymmetrical, but switching the peptides between the two different ends of the linker (head to head or head to tail) had little effect on binding nor did substituting a variety of small labels (5-carboxyfluorescein, biotin, or chelates) at the position indicated in Figure 5. One might expect that serendipity as regards the linker length was responsible for the overall success, but in limited experiments linker length also was not important between 20−40 atoms.

Tyrosine kinases are known to dimerize in vivo during activation. In fact, the activating ligand, VEGF, is itself a dimer that appears to bind between two tyrosine kinase monomer

SCHEME 1. Binding of Hetero-bivalent Peptides to VEGF-R2[a]

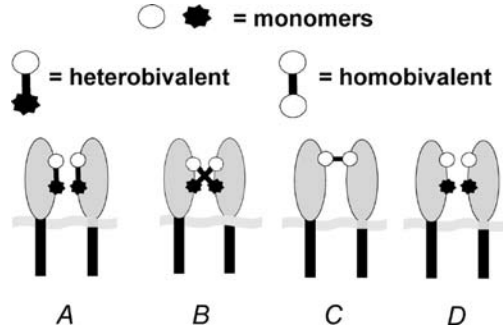

[a] Diagram A is the probable binding mode for hetero-bivalents to VEGF-R2.

units.[18] We hypothesize that the probable mode of binding is for our hetero-bivalent molecules to bind to only one monomer unit of VEGF-R2, competing with VEGF binding and also the dimerization critical for phosphorylation (diagram A, Scheme 1). If the hetero-bivalents were binding across the VEGF-R2 dimer (diagram B, Scheme 1), we would expect both monomer mixtures of the two peptides and the homo-bivalents with low K_d values (diagrams C and D, Scheme 1) to be competitive with hetero-bivalents and with VEGF in the activation assays.

Since the molecules in question are not very sensitive to labeling and are small, highly active binders, the primary goal of the study was achieved. Apparently, at least as far as tyrosine kinases are concerned, the procedure used is

generally useful. It is possible that the phenomenon could be further generalized to proteins other than tyrosine kinases. These types of constructs are now being used to generate molecular imaging diagnostics for eventual clinical testing as anti-angiogenesis and other agents.

Targeted US Agents

Ultrasound imaging contrast agents are 2 μm diameter spheres, the inside of which is filled with an aqueous insoluble gas such as SF_6 or fluorocarbons. The bubble shell is usually made up of monolayer phospholipids that can be labeled with targeting entities through biotin−avidin interactions or with target ligands bearing lipids that adhere to the lipophilic bubble surface.[19] To attach peptides we created phospholipid−linker−peptide conjugates, as reported by von Wronski et al.[20] Theoretically, ~50 bubbles can adhere to a single endothelial cell on the luminal side of a blood vessel, and probably groups of about 10−20 can be visualized in a static US image. When in motion, even a single bubble can be seen against a static background, making US contrast agent imaging competitive even with nuclear medicine in sensitivity. Our objective was to create a bubble targeted to an angiogenesis target that existed on the intraluminal surface of blood vessel endothelial cells. This is a necessary target location restriction of large entities like US bubbles.

For targeting ligands, we planned a campaign as in the hetero-bivalent project. We chose the peptide TKPPR as a nonbinding control because it existed in quantity in our laboratory. TKPPR was available because we had researched a ^{99m}Tc(R-TKPPR)[21] molecule (RP-128) for diagnostically targeting inflammation. TKPPR is an antagonist derived from TKPR, a fragment of the Fc region in IgG antibodies named tuftsin by its discoverers. The tuftsin receptor is thought to be involved in the primary events in inflammation, binding to a structurally uncharacterized tuftsin receptor expressed on monocyte-derived macrophages. While tuftsin had been known and studied for over 30 years, the receptor had not been sequenced or cloned.

Phospholipid constructs (Figure 6a) were synthesized and incorporated into bubbles by mixing, creating constructs with 1−5% of the surface lipid as lipid−peptide. Thus hundreds of bubble-attached binders can act simultaneously when the targeted bubble binds to a cell.

Cultured endothelial cells express angiogenesis receptors without the need for stimulation or artificial gene upregulation, so we used a cultured human endothelial cell screen as a first test for binding of targeted bubbles to angiogenesis receptors. The bubbles were suspended and added to the cultured cells growing on the bottom of a transparent container. When the container was inverted the bubbles floated, contacting the cells. Then they were reinverted, washed, and counted by light microscopy. Figure 7 shows light micrographs of human endothelial cells in confluent culture after incubation with ultrasound bubbles. The underivatized bubbles do not bind the cells, while the TKPPR-derivatized bubbles, the "negative" control, do bind the cells. Incubation of the TKPPR bubbles with free TKPPR inhibited the binding, suggesting a specific binding interaction with a weak but significant IC_{50} of 12.5 μM for the monomeric TKPPR competing with highly multimeric TKPPR bubbles. Noting that VEGF's last exon, exon 8, ends in the sequence, KPRR at the C terminus, VEGF was tested against the TKPPR bubbles, and it successfully competed the TKPPR bubbles off the endothelial cells with IC_{50} = 0.3 nM.

Table 3 records a series of experiments used to elucidate a mechanism for the interaction. The $(TKPPR)_2$ and $(TKPPR)_4$ entities are synthetic homo-bivalent and a homo-tetravalent constructs of TKPPR labeled with fluorescent Oregon Green[22] (Figure 6b). Multivalency effects account for the differing binding strengths in rows 6 and 7. TKPR is a weaker binder than TKPPR and weaker at inhibiting TKPPR-bubble binding to the endothelial cells, while $(TKPPR)_4$ has IC_{50} 125 times lower.

BSA, heparin, IgG, bFGF, PlGF-1, IL-1, the cyclic peptide CTKPPRC, and finally $VEGF_{121}$ were all negative and did not block the TKPPR bubble binding. The negative results pointed to a specific reaction. $VEGF_{121}$ differs from VEGF ($VEGF_{165}$ herein) in that it lacks exon 7 that codes for a region of VEGF associated with binding a co-receptor, neuropilin-1 (NP-1). This suggested that NP-1 was the target of the multivalent bubbles. To validate this hypothesis, ^{125}I-VEGF was allowed to bind to NP-1/Fc fusions in the presence of potential inhibitors (rows 8−11, Table 4). The reaction was inhibited at 100 nM for the tetramer, which also bound to NP-1/Fc fusions at 25−50 nM (rows 12 and 13, Table 4). Biological activity was demonstrated by autophosphorylation and other experiments.[23]

Exon 7 in VEGF is necessary for NP-1 binding, but the purpose of exon 8, which codes only for the amino acids CDKPRR, had never been reported. Our experiments suggest that exon 8 of VEGF is involved in NP-1 binding and that the related peptides, TKPPR and its multimers, interfere with that binding. These conclusions were quickly validated and used by experimenters in other laboratories.[24−26] It is indeed possible that most, if not all, the activity of tuftsin is accounted for

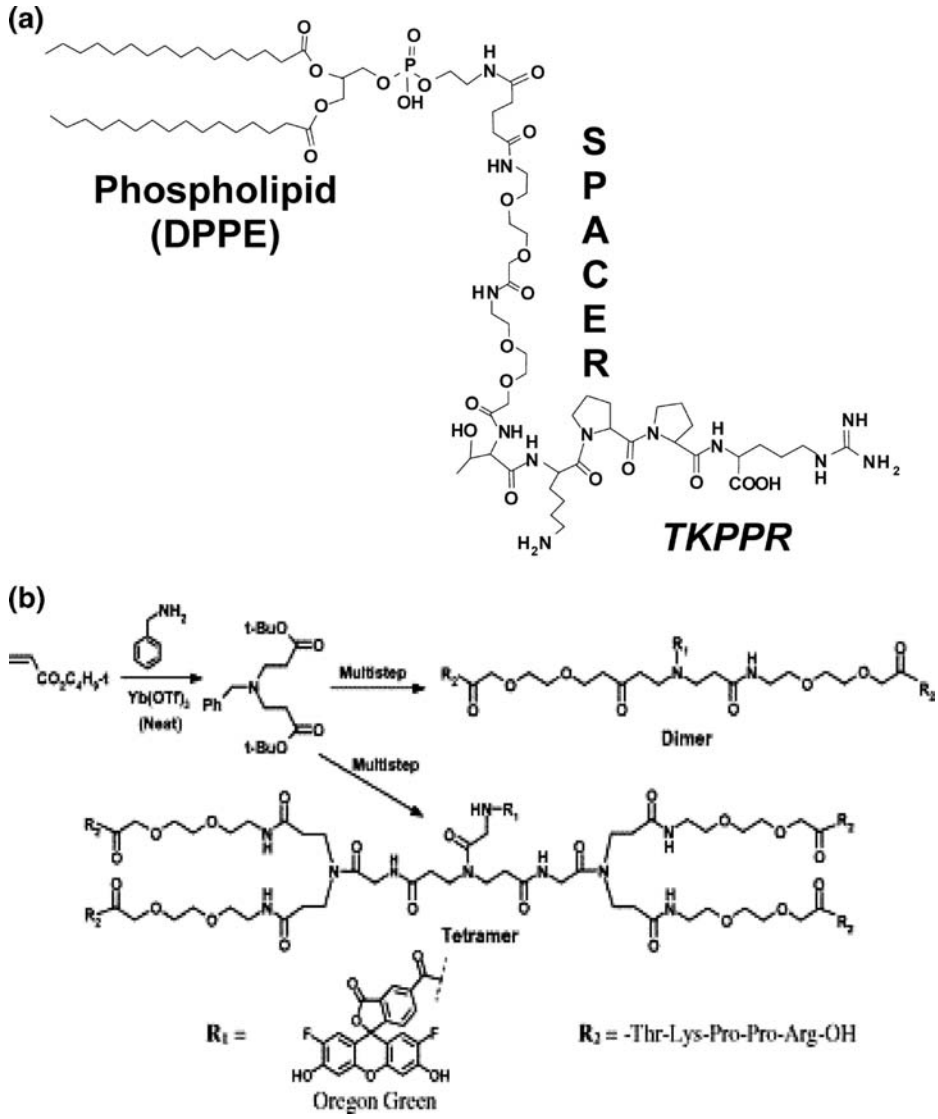

FIGURE 6. Structures of (A) TKPPR-derivatized phospholipid used to label ultrasound bubbles and (B) the synthetic tetravalent TKPPR ligands.

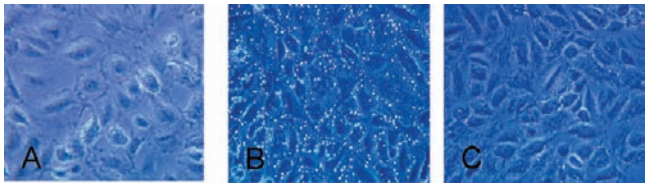

FIGURE 7. Light micrographs of cultured human endothelial cells incubated with ultrasound bubbles:[20] (A) underivatized bubbles; (B) TKPPR-derivatized bubbles; (C) TKPPR-derivatized bubbles mixed with 100 μM TKPPR.

by NP-1. It is in fact possible that the tuftsin receptor, in whole or part, *is* NP-1.

Recently, we demonstrated that a radiolabeled tetrameric TKPPR molecule accumulated rapidly and substantially (5.2% ID/g at 1 h) in a receptor-positive mouse xenograft model (PC-3 tumors) with low uptake in most other tissues excluding the kidneys.[27] We also used fluorescent Qdots with thioacetyl-derivatized TKPPR tetramers (made as in Figure 6) to probe confluent endothelial cells in culture. Both the TKPPR monomer and an anti-NP-1 antibody blocked the binding, demonstrating specificity of multivalent TKPPR for the NP-1 receptor.[28] The work also showed that while the Qdots were initially bound strongly at the cell's lateral edges at cell−cell junctions, after 1 h at 37 °C, they internalized and migrated toward the nucleus (Figure 8). Temperature of 4 °C inhibits the process suggesting an active endocytosis and a therapeutic potential for this receptor−ligand combination, in addition to the obvious diagnostic one in angiogenesis.

There is one downside to of the power of multivalency to enhance binding in larger constructs like the US bubbles. A very small amount of specific binding to an unintended target could be undetectable in phage screening campaigns but well detected or even dominant after the

TABLE 4. K_d and IC_{50} Results for TKPPR-Targeted Entities[20] [a]

no.	compound	target	competitor	K_d	IC_{50}	method
1	bubble	EC[b]	none			light microscopy
2	TKPPR bubble	EC	none			light microscopy
3	TKPPR bubble	EC	TKPPR		12.5 μM	light microscopy
4	TKPPR bubble	EC	VEGF		0.3 nM	light microscopy
5	TKPPR bubble	EC	TKPR		100 μM	light microscopy
6	TKPPR bubble	EC	TKPPR		12.5 μM	light microscopy
7	TKPPR bubble	EC	$(TKPPR)_4$		100 nM	light microscopy
8	^{125}I-VEGF	NP-1/Fc	VEGF		1.5 nM	radioactivity
9	^{125}I-VEGF	NP-1/Fc	TKPPR		30 μM	radioactivity
10	^{125}I-VEGF	NP-1/Fc	$(TKPPR)_2$		3 μM	radioactivity
11	^{125}I-VEGF	NP-1/Fc	$(TKPPR)_4$		100 nM	radioactivity
12	$(TKPPR)_4$	VEGF-R2/Fc		none		fluorescence polarization
13	$(TKPPR)_4$	NP-1/Fc		25−50 nM		fluorescence polarization

[a] Reprinted in part with permission from ref 23. [b] Cultured endothelial cell.

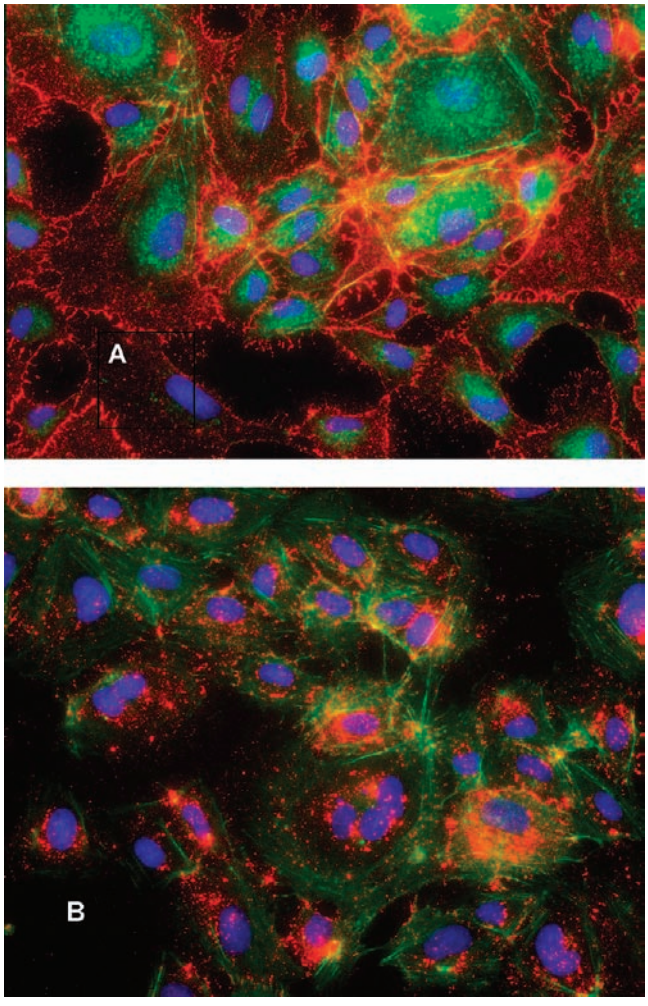

FIGURE 8. TKPPR Qdot (red) (A) binding to confluent HUVEC cells at 4 °C and (B) internalization by HUVEC cells after 1 h at 37 °C after prebinding at 4 °C. Green = phalloidin−Oregon Green staining of the cytoskeleton (400× magnification). Blue structures are stained nuclei.[27,28]

binding peptides work in the highly multivalent format on a bubble. The same effect could be anticipated for other nanoparticles.

Conclusions

Small peptides can be effective choices as targeting ligands. In diagnostic imaging, this allows rapid background clearance. In systemic radiotherapy, rapid blood clearance, relative to antibodies, offers the advantages of reduced bone marrow radiotoxicity via reduced exposure of bone marrow to circulating drug and greater tumor uptake from greater administered doses. When natural peptides are unavailable, they can be effectively created de novo for some important isolable targets and subsequently enhanced to nanomolar or subnanomolar binding strengths by multimerization techniques, resulting in targeted molecular imaging agent ligands of high specificity and binding strength. The technique described herein was especially effective and resulted in relatively small binding constructs (<5 kDa) with unusually strong binding (K_d < 1 nM). The finding opens the possibility of new targeted diagnostic imaging agents and generalization to other receptor families. Bound to US bubbles, even weak-binding peptides can target at high avidity due to a powerful multivalency effect.

The author thanks his former colleagues for their scientific collaboration and for review of this manuscript and the Bracco Group for their consistent and generous support of imaging research.

BIOGRAPHICAL INFORMATION

Dr. Michael Tweedle (b. 1951, Vincennes, Indiana) was educated at Knox College (B.A.), Rice University (Ph.D.), and Stanford University. He has held industrial research positions at New England Nuclear, DuPont, Squibb, and Bristol-Myers-Squibb and was President of Bracco Research USA. He is currently Professor of Radiology at The Ohio State University where he holds The Stefanie Spielman Chair in Cancer Imaging.

REFERENCES

1 Tweedle, M. F.; Gaughan, G.; Hagan, J. 1-Substituted-1,4,7, triscarboxymethyl-1,4,7,10-tetraazacyclododecane and analogs. U.S. Patent No. 4,885,363, 1989.

2 Gries, H.; Rosenberg, D.; Weinman, H.-J. Diagnostic media. U.S. Patent No. 4,647,447, 1987.

3 Desreux, J. F.; Loncin, M. F.; Spirlet, M. R. Solution and solid state structures of lanthanide complexes with polyaza polyacetic macrocyclic ligands: A comparison of NMR and X-ray studies. *Inorg. Chim. Acta* **1984**, *94*, 43.

4 Cacheris, W. P.; Nickle, S. K.; Sherry, A. D. Thermodynamic study of lanthanide complexes of 1,4,7-triazacyclononane-*N,N′,N″*-triacetic acid and 1,4,7,10-tetraazacyclododecane-*N,N′,N″,N‴*-tetraacetic acid. *Inorg. Chem.* **1987**, *26*, 958–960.

5 Merbach, A. E., Toth, E., Eds. *The Chemistry of Contrast Agents in Medical Magnetic Resonance Imaging*; Wiley: New York, 2001.

6 Unfortunately, DOTA and DO3A are used often used interchangeably. DOTA should be used for tetra-acetates and DO3A for triacetates.

7 (a) Lantry, L. E.; Cappeletti, E.; Maddalena, M.; Fox, J. S.; Feng, W.; Chen, J.; Thomas, R.; Eaton, S. M.; Bogdan, N. J.; Arunachalam, T.; Reubi, J. C.; Raju, N.; Kattuada, L.; Linder, K. E.; Swenson, R. E.; Tweedle, M. F.; Nunn, A. D. LuAMBA: Synthesis and characterization of a selective ^{177}Lu-labeled GRP-R agonist for systemic radiotherapy of prostate cancer. *J. Nucl. Med.* **2006**, *47*, 1144–1152. (b) Chen, J.; Linder, K. E.; Cagnolini, A.; Metcalfe, E.; Raju, N.; Tweedle, M. F.; Swenson, R. E. Synthesis, stabilization and formulation of [^{177}Lu]Lu-AMBA, a systemic radiotherapeutic agent for gastrin releasing peptide receptor positive tumors. *Appl. Radiat. Isotopes* **2008**, *66*, 497–505. (c) Waser, B.; Eltschinger, V.; Linder, K.; Nunn, A.; Reubi, J. C. Selective in vitro targeting of GRP and NMB receptors in human tumours with the new bombesin tracer 177Lu-AMBA. *Eur. J. Nucl. Med. Mol. Imaging* **2007**, *34*, 95–100. (d) Panigone, S.; Nunn, A. D. Luttetium-177-labeled gastrin releasing peptide receptor binding analog: a novel approach to radionuclide therapy. *Q. J. Nucl. Med. Mol. Imaging* **2006**, *50*, 310–321. (e) Thomas, R.; Chen, J.; Roudier, M. M.; Vessella, R. L.; Lantry, L. E.; Nunn, A. D. In vitro binding evaluation of ^{177}Lu-AMBA, a novel ^{177}Lu-labeled GRP-R agonist for systemic radiotherapy in human tissues. *Clin. Exp. Metastasis* **2009**, *26*, 105–119.

8 Swenson, R. E.; Lattuada, L.; Linder, K. E.; Capalleti, E.; Raju, N.; Chen, J.; Lantry, L. E.; Thoma, R.; Arunachalum, T.; Maddelena, M. E.; Fox, J. S.; Nunn, A. D. Tweedle, M. F. Optimization of the linker between the metal chelate and the targeting peptide provided the superior properties of 177Lu-AMBA, a GRP radiotherapeutic in clinical development, Presented at the 236th ACS meeting, 2008, abstract no. 387.

9 Smith, C. J.; Gali, H.; Sieckmanc, G. L.; Hayesb, D. L.; Owenb, N. K.; Mazurub, D. G.; Volkert, W. A.; Hoffman, T. J. Radiochemical investigations of ^{177}Lu-DOTA-8-Aoc-BBN[7−14]NH2: An in vitro/in vivo assessment of the targetingability of this new radiopharmaceutical for PC-3 human prostate cancer cells. *Nucl. Med. Biol.* **2003**, *30*, 101–109.

10 Linder, K. E.; Metcalfe, E.; Arunachalam, T.; Chen, J.; Eaton, S. M.; Feng, W.; Fan, H.; Raju, N.; Cagnolini, A. In vitro and in vivo metabolism of Lu-AMBA, a GRP-receptor binding compound and the synthesis and characterization of its metabolites. *Bioconjugate Chem.*, in press.

11 Bodei, L.; Ferrari, M.; Nunn, A.; Llull, J. B.; Cremonesi, M.; Martano, L.; Laurora, G.; Scardino, E.; Tiberini, S.; Bufi, G.; Eaton, S.; De Cobelli, O.; Paganelli, G. Presented at the European Association for Nuclear Medicine meeting, 2007, Copenhagen.

12 Cagnolini, A.; Metcalfe, E.; Nguyen, H.; Swenson, R. E.; Linder, K. E. Isolation of a ^{177}Hf complex formed by β-decay of a ^{177}Lu-labeled radiotherapeutic compound and NMR structural elucidation of the ligand and its Lu and Hf complexes. *Inorg. Chem.* **2009**, *48*, 3114–3124.

13 Kumar, K.; Tweedle, M. F. Ligand basicity and rigidity control formation of macrocyclic polyaminocarboxylate complexes of Gd(lll). *Inorg. Chem.* **1993**, *32*, 4193–4199.

14 Sato, A. K.; Sexton, D. J.; Morganelli, L. A.; Cohen, E. H.; Wu, Q. L.; Conley, G. P.; Streltsova, Z.; Lee, S. W.; Devlin, M.; DeOliveira, D. B.; Enright, J.; Kent, R. B.; Wescott, C. R.; Ransohoff, T. C.; Ley, A. C.; Ladner, R. C. *Biotechnol. Prog.* **2002**, *18*, 182–192. Enright, J.; Kent, R. B.; Wescott, C. R.; Ransohoff, T. C.; Ley, A. C.; Ladner, R. C. Development of mammalian serum albumin affinity purification media by peptide phage display. *Biotechnol. Prog.* **2002**, *18*, 182–192.

15 Ellis, L. M.; Hicklin, D. J. VEGF-targeted therapy: mechanisms of anti-tumour activity. *Nat. Rev. Cancer* **2008**, *8*, 579–591.

16 Shrivastava, A.; von Wronski, M.; Sato, A. K.; Dransfield, D. T.; Sexton, D.; Bogdan, N.; Pillai, R.; Nanjappan, P.; Song, B.; Marinelli, M.; DeOliveira, D.; Luneau, C.; Devlin, D.; Muruganandam, M.; Abujoub, A.; Connelly, G.; Wu, Q.; Conley, G.; Chang, Q.; Tweedle, M. F.; Ladner, R. C.; Swenson, R. E.; Nunn, A. D. A distinct strategy to generate high-affinity peptide binders to receptor tyrosine kinases. *Protein Eng., Des. Sel.* **2005**, *18*, 417–424.

17 Pillai, R.; Marinelli, E. R.; Swenson, R. E. A flexible method for preparation of peptide homo- and heterodimers functionalized with affinity probes, chelating ligands, and latent conjugating groups. *Pept. Sci.* **2006**, *84*, 576–585.

18 Wiesmann, C.; Fuh, G.; Christinger, H. W.; Eigenbrot, C.; Wells, J. A.; de Vos, A. M. Crystal Structure at 1.7 Å Resolution of VEGF in Complex with Domain 2 of the Flt-1 Receptor. *Cell* **1997**, *91*, 695–704.

19 (a) Klibanov, A. L. Targeted delivery of gas-filled microspheres, contrast agents for ultrasound imaging. *Adv. Drug Delivery Rev.* **1999**, *37*, 139–157. (b) Klibanov, A. L. Ultrasound molecular imaging with targeted microbubble contrast agents. *J. Nucl. Cardiol.* **2007**, *14*, 876–884.

20 von Wronski, M.; Raju, N.; Pillai, R.; Bogdan, N. J.; Marinelli, E. R.; Nanjappan, P.; Ramalingam, K.; Arunachalam, T.; Eaton, S.; Linder, K.; Yan, F.; Pochon, S.; Nunn, A. D.; Tweedle, M. F. Tuftsin binds neuropilin-1 through a sequence similar to that encoded by exon 8 of VEGF. *J. Biol. Chem.* **2006**, *281*, 5702–5710.

21 Caveliers, V.; Goodbody, A. E.; Tran, L. L.; Peers, S. H.; Thornback, J. R.; Bossuyt, A. Evaluation of ^{99m}Tc-RP128 as a potential inflammation imaging agent: Human dosimetry and first clinical results. *J. Nucl. Med.* **2001**, *42*, 154–161.

22 Raju, N.; Ranganathan, R. S.; Tweedle, M. F.; Swenson, R. E. A new dendrimer scaffold for preparing dimers or tetramers of biologically active molecules. *Tetrahedron Lett.* **2005**, *46*, 1463–1465.

23 Tweedle, M. F. Adventures in multivalency - The Harry Fischer Memorial Lecture. *Contrast Media Mol. Imaging* **2006**, *1*, 2–9.

24 Vander Kooi, C. W.; Jusino, M. A.; Perman, B.; Neau, D. B.; Bellamy, H. D.; Leahy, D. J. Structural basis for ligand and heparin binding to neuropilin B domains. *Proc. Natl. Acad. Sci. U.S.A.* **2007**, *104*, 6152–6157.

25 Geretti, E.; Shimizu, A.; Klagsbrum, M. Neuropilin structure governs VEGF and semaphorin binding and regulates angiogenesis. *Angiogenesis* **2008**, *11*, 31–39.

26 Pan, Q.; Chathery, Y.; Wu, Y.; Rathore, N.; Tong, R. K.; Peale, F.; Bagri, A.; Tessier-Lavigne, M.; Koch, A. W.; Watts, R. Neuropilin-1 binds to $VEGF_{121}$ and regulates endothelial cell migration and sprouting. *J. Biol. Chem.* **2007**, *282*, 24049–24052.

27 von Wronski, M.; Raju, N.; Bogdan, N. J.; Fox, J.: Lantry, L. E.; Tweedle, M. F.; Nunn, A. D. Anti-neuropilin-1 antibodies block the binding of a tuftsin-antagonist peptide, TKPPR, to neuropilin-1 in mice and on receptor-positive cells, Presented at the Joint Molecular Imaging Conference, 2007, abstract no. 0164.

28 Von Wronski, M.; Raju, N.; Tweedle, M. F.; Nunn, A. D. Subcellular localization of neuropilin-1 on endothelial cells with peptide-targeted quantum dots, Presented at the American Association for Cancer Research meeting, 2008, abstract no. LB-197.